**RAA 2016** Vol. **16** No. **6**, 94 (6pp) doi: 10.1088/1674–4527/16/6/094
*http://www.raa-journal.org* *http://iopscience.iop.org/raa*

***R**esearch in*
***A**stronomy and*
***A**strophysics*

# Lunar-based Ultraviolet Telescope study of the well-known Algol-type binary TW Dra

Wen-Ping Liao[1,2], Sheng-Bang Qian[1,2,3], Miloslav Zejda[4], Li-Ying Zhu[1,2,3] and Lin-Jia Li[1,2]

[1] Yunnan Observatories, Chinese Academy of Sciences, Kunming 650216, China; *liaowp@ynao.ac.cn*
[2] Key Laboratory of the Structure and Evolution of Celestial Objects, Chinese Academy of Sciences, Kunming 650216, China
[3] University of Chinese Academy of Sciences, Beijing 100049, China
[4] Department of Theoretical Physics and Astrophysics, Masaryk University, Kotlářská 2, CZ-611 37 Brno, Czech Republic

Received 2015 November 5; accepted 2016 February 3

**Abstract** By using the Lunar-based Ultraviolet Telescope (LUT) from 2014 December 2 to December 4, the first near-UV light curve of the well-known Algol-type binary TW Dra is reported, which is analyzed with the 2013 version of the W-D code. Our solutions confirmed that TW Dra is a semi-detached binary system where the secondary component fills its Roche lobe. The mass ratio and a high inclination are obtained ($q = 0.47$, $i = 86.68°$). Based on 589 available data spanning more than one century, the complex period changes are studied. Secular increase and three cyclical changes are found in the corresponding orbital period analysis. The secular increase changes reveal mass transfer from the secondary component to the primary one at a rate of $6.8 \times 10^{-7}\ M_\odot\ \mathrm{yr}^{-1}$. One large cyclical change of 116.04 yr may be caused by disturbance of visual component ADS 9706B orbiting TW Dra (ADS 9706A), while the other two cyclical changes with shorter periods of 22.47 and 37.27 yr can be explained as the result of two circumbinary companions that are orbiting around TW Dra, where the two companions are in simple $3 : 5$ orbit-rotation resonances. TW Dra itself is a basic binary in a possible sextuple system with the configuration $(1 + 1) + (1 + 1) + (1 + 1)$, which further suggests that multiplicity may be a fairly common phenomenon in close binary systems.

**Key words:** stars: binaries: close — stars: binaries: eclipsing — stars: individual (TW Draco)

## 1 INTRODUCTION

The variability of Algol-type TW Dra was discovered in 1910 (Pickering 1910). It is an Algol-type system with a $\delta$ Scuti-like oscillating primary component (Zhang et al. 2013), and it is the A-component of the visual binary ADS 9706. Detailed spectroscopic and photometric investigations of TW Dra have been published since its discovery, e.g., Baglow (1952); Walter (1978); Giuricin et al. (1980); Papoušek et al. (1984); Smith (1949); Popper (1989); Qian & Boonrucksar (2002); Zejda et al. (2008); Tkachenko et al. (2010); Zejda et al. (2010); Bozic et al. (2013). A historical summary of the investigation was given in Tkachenko et al. (2010) and Zejda et al. (2008). Here, we will focus on several studies of TW Dra in recent years. Tkachenko et al. (2010) investigated this system in detail based on high-resolution spectra, and derived reliable orbital elements: $M_1 = 2.2(\pm0.1)M_\odot$, $M_2 = 0.90(\pm0.05)M_\odot$, $a = 12.2(\pm0.2)R_\odot$, $T_1 = 8160(\pm15)$ K, $q = 0.411(\pm0.004)$, $i = 86.8°(\pm0.3°)$. Orbital period changes in TW Dra have been studied by many researchers. Rather complicated changes of the orbital period were studied in detail by Zejda et al. (2008), who also summarized previous studies on this topic. They analyzed $(O - C)$ curves in two stages, e.g., 1858–1942 and 1942–2007. A period increase and a small cyclical 6.5-year variation were found. Based on multicolor light curves, Zejda et al. (2010) and Bozic et al. (2013) derived similar solutions of TW Dra by using the PHOEBE program. Zejda et al. (2010) pointed out that this system could be a quadruple system. In the new solution of Bozic et al. (2013), they mentioned that the small variation with a period of 6.5 yr in the system proposed by Wolf (1990) and Zejda et al. (2008) is not sufficient to explain the large discrepancy between the observed and expected value of the period. In view of this reason and more new data that have been collected, we reproduce and investigate the $(O - C)$ diagram. According to Cao et al. (2011), the variation of brightness in the near-ultraviolet (near-UV) band is normally much stronger than in other bands. TW Dra is a binary system with large brightness variations in the near-UV band, therefore, TW Dra was targeted for observations by the Lunar-

based Ultraviolet Telescope (LUT). Section 2 gives LUT observations of TW Dra. Section 3 describes photometric solutions of LUT light curves. Section 4 shows orbital period analysis of TW Dra. Section 5 gives conclusions and discussion.

## 2 LUNAR-BASED ULTRAVIOLET TELESCOPE OBSERVATIONS

TW Dra was observed from 2014 December 2 to December 4 by using LUT, which has an aperture of 15 cm and covers a range in the near-UV band of 245∼340 nm. The field of view is $1.27^\circ \times 1.27^\circ$. The detectable stellar magnitude limit is 13 mag (Wen et al. 2014; Cao et al. 2011). The photometric performance of LUT was shown to be highly stable during its first six months of operation (Wang et al. 2015).

By using the data processing method of Meng et al. (2015), two eclipse light curves were obtained and are plotted in Figure 1. By using a least squares parabolic fitting method, two times of light minima,

$$\mathrm{Min\,I} = 2456994.45291 \pm 0.00045\,,$$

and

$$\mathrm{Min\,II} = 2456995.86490 \pm 0.00542\,,$$

were determined. The near-UV phased light curve is displayed in Figure 2. The phases were calculated with the equation 2456994.45291+$2.806854^{\mathrm{d}} \times E$ (where $2.806854^{\mathrm{d}}$ is taken from the $O-C$ gateway: *http://var.astro.cz/ocgate*).

## 3 THE ANALYSIS OF LIGHT CURVES

The near-UV light curve was analyzed using the 2013 version of the W-D code (Wilson & Devinney 1971; Wilson 1979, 1990; Van Hamme & Wilson 2007; Wilson 2008; Wilson et al. 2010; Wilson 2012). The temperature for star 1 (star eclipsed at primary minimum light) was fixed at $T_1 = 8160$ K during the analysis (Tkachenko et al. 2010). Considering that spectral type for the primary component was classified as A5V while the secondary component is a K0-type giant (Tkachenko et al. 2010), the gravity-darkening coefficients $g_1 = 1.0, g_2 = 0.32$ and the bolometric albedo $A_1 = 1.0, A_2 = 0.5$ were chosen for the two component stars. For the bolometric and bandpass limb-darkening coefficients, an internal computation based on the result of van Hamme (1993) with the logarithmic law was used. The solutions converged at mode 5 (semi-detached with star 2 filling its limiting lobe).

Because TW Dra is the brighter member (ADS 9706A) of the visual binary ADS 9706, the light contribution from the fainter one (ADS 9706B) should be considered. Two models (with and without a third light) were used during our analysis. A q-search method was used to determine the mass ratio. The best solutions were found near $q = 0.60$ without a third light and $q = 0.47$ with a third light. The value $q = 0.47$ is closer to the spectral value obtained by Tkachenko et al. (2010), and the corresponding relation between the resulting weighted sum of squared deviations $\Sigma$ and the mass ratio $q$ is plotted in Figure 3. Then, we expanded the number of adjustable parameters beyond just the mass ratio and started iterations with the initial values of $q = 0.60$ and $q = 0.47$. Iterations were performed until convergence. The final solutions for the two cases were derived. The solid lines in Figure 2 show the theoretical light curves with and without a third light. It can be seen from this figure that the difference in fitting is mainly near the primary eclipse. Considering the fact that the primary eclipse is total (Popper 1989), we take the photometric solutions with the third light as our final solutions, which are listed in Table 1.

**Table 1** Photometric Solutions of TW Dra

| Parameter | Solutions with third light |
|---|---|
| mode | 5 |
| $i$ [°] | 86.684 (±0.397) |
| $q\,[m_2/m_1]$ | 0.4749 (±0.0073) |
| $T_1$ [K] | 8160 |
| $T_2$ [K] | 5331 (±26) |
| $\Omega_1$ | 5.00307 (±0.04847) |
| $\Omega_2$ | 2.82728 |
| $L_1/(L_1+L_2)$ (UV) | 0.9436 (±0.0002) |
| $L_2/(L_1+L_2)$ (UV) | 0.0564 (±0.0002) |
| $L_3/(L_1+L_2+L_3)$ (UV)(%) | 7.1 (±0.3) |
| $r_1$ (pole) | 0.2207 (±0.0022) |
| $r_1$ (side) | 0.2224 (±0.0022) |
| $r_1$ (back) | 0.2240 (±0.0023) |
| $r_2$ (pole) | 0.2963 (±0.0012) |
| $r_2$ (side) | 0.3091 (±0.0013) |
| $r_2$ (back) | 0.3417 (±0.0013) |
| $\Sigma \mathrm{res}^2$ | $0.24\times10^{-5}$ |

## 4 COMPLEX ORBITAL PERIOD CHANGES OF TW DRA

By combining data listed in table 1 of Zejda et al. (2008) with those acquired after 2008, we compiled a total of 589 data points. Using these data, the orbital period changes were re-analyzed by us. Due to their large scatters, values for HJDs 2399833.429, 2404663.296 and 2441395.467 were not used in our analysis. The $(O-C)$ values were computed with the linear ephemeris given by the $(O-C)$ gateway,

$$\mathrm{Min\,I} = 2433310.238 + 2.806854^{\mathrm{d}} \times E. \quad (1)$$

The top panel of Figure 4 shows the corresponding $(O-C)$ curve, where open circles refer to low-precision observations (i.e., visual or photographic data), and filled circles refer to high-precision observations (i.e., photoelectric or CCD data). As shown in this panel, the orbital period changes of this star are complicated. Generally, a pattern of a cyclic variation + a long-term change exists. Therefore, during our analysis process, we first try to use

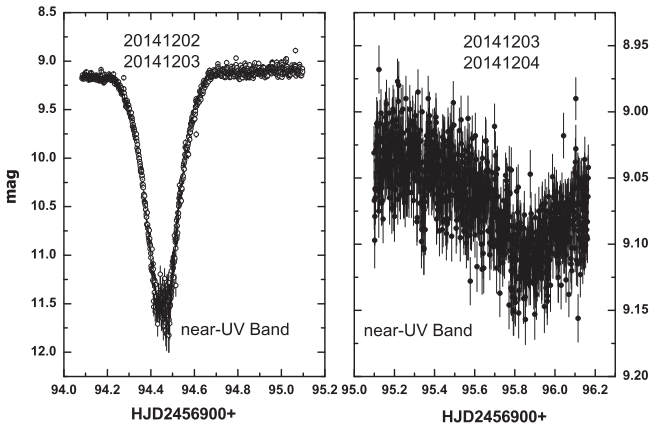


**Fig. 1** Near-UV light curves of TW Dra obtained with the LUT from 2014 December 2 to December 4. Open and filled circles represent light curves of primary and secondary minima observations, respectively.

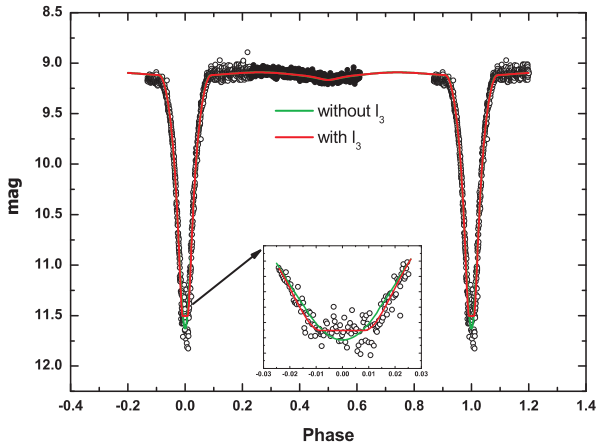


**Fig. 2** The observed and theoretical near-UV light curves (*solid lines*) of TW Dra. The green line is calculated without a third light while the red line is calculated with a third light. The symbols are the same as those in Fig. 1.

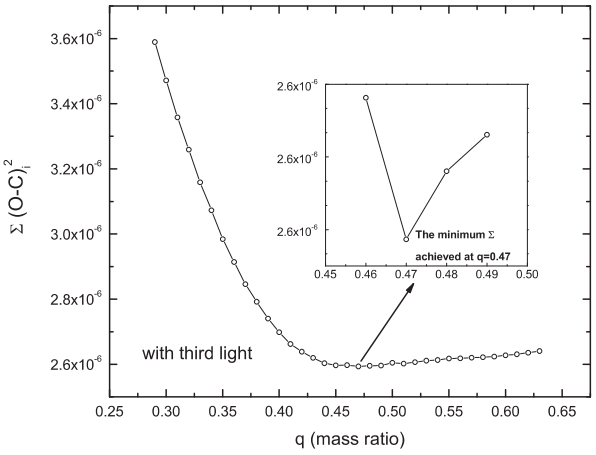


**Fig. 3** Relation between the resulting weighted sum of squared deviations $\Sigma$ and the mass ratio $q$ determined with a third light.

parabolic-plus-one cyclic variation to fit the general trend of the $(O-C)$ changes. Weights of 1 and 10 were applied to low-precision observations and high-precision observations, respectively. Then, based on the least-squares method, the following equation was obtained

$$O-C = \Delta JD_0 + \Delta P_0 E + \frac{\beta}{2}E^2 + A\sin(\Omega E + \phi), \quad (2)$$

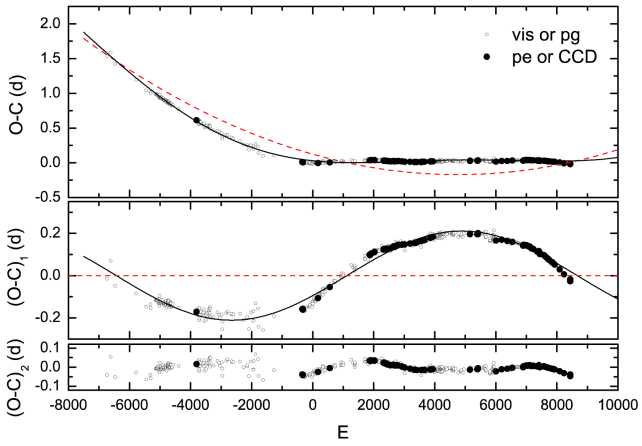


**Fig. 4** *Top panel*: $(O-C)$ curve of TW Dra calculated with Eq. (1). The solid line refers to a combination of a secular increase and a cyclic period variation, and the dashed line to a quadratic fit. *Middle panel*: residuals after removal of the parabolic fit and its least-squares fit by a sinusoidal equation (*solid line*). *Bottom panel*: the residuals from Eq. (2). The open and filled circles refer to visual or photographic data and photoelectric or CCD ones, respectively.

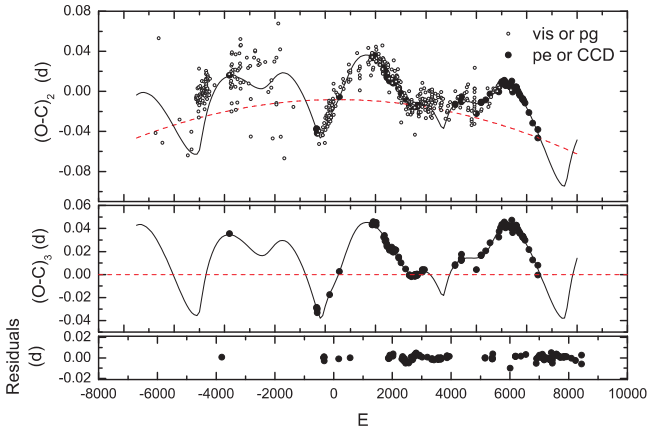


**Fig. 5** *Top panel*: The $(O-C)_2$ diagram shows the residuals from the fitting performed in the first step. The solid line refers to a combination of a quadratic and two cyclical variations with eccentricity. The downward parabolic change here could be considered as a small correction to the upward parabolic change seen in the first step. *Middle panel*: $(O-C)_3$ curve of TW Dra described by the $\tau_4$ and $\tau_5$ terms of Eq. (3) (*solid line*), after removing the other terms. *Bottom panel*: the residuals from Eqs. (3)–(5).

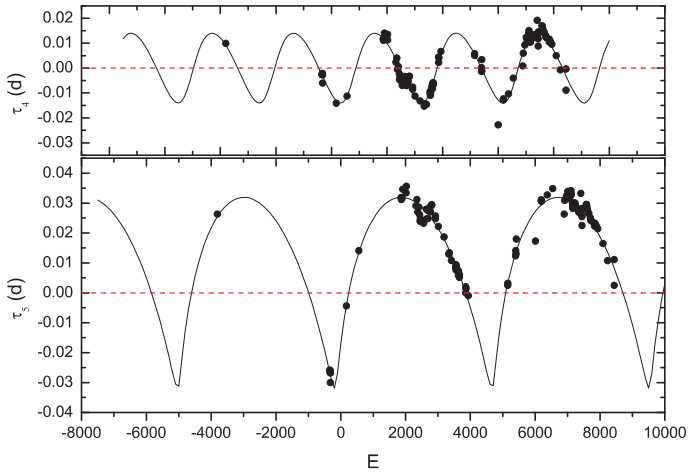


**Fig. 6** Two periodic variations with eccentricities of 0.29 (*top panel*) and 0.81 (*bottom panel*).

**Table 2** Parameters Describing the Orbits of Potential Additional Bodies in the TW Dra System

| Parameters | Parabolic-plus-one pure cyclic variation | Parabolic-plus-two cyclic variations with eccentricity (Step 2) | |
|---|---|---|---|
| | (Step 1) | $\tau_4$ | $\tau_5$ |
| $\Delta JD_0$ (HJD) | 0.1252(50) | –0.0084(41) | –0.0084(41) |
| $\Delta P_0$ (d) | –0.0001239(39) | 0.00000059(±60) | 0.00000059(±60) |
| $P_3$ (yr) | 116.04±3.55 | 22.47±0.29 | 37.27±0.41 |
| $\Omega$ (°) | 0.0238±0.0007 | – | – |
| $\phi$ (°) | 333±2 | – | – |
| $\omega$ (°) | – | 332±10 | 298±10 |
| $\beta$ (d cycle$^{-1}$) | (2.61±0.06)×10$^{-8}$ | (–1.20±0.13)×10$^{-9}$ | (–1.20±0.13)×10$^{-9}$ |
| $e$ | – | 0.29±0.06 | 0.81±0.14 |
| $A$ (d) | 0.2108±0.0136 | 0.0145±0.0005 | 0.0346±0.0068 |
| $T$ (HJD) | – | 2443499.0±240.8 | 2446536.0±224.1 |
| $a_{12}\sin i_3$(AU) | 36.52±2.36 | 2.51±0.09 | 5.99±1.18 |
| $f(m)(M_\odot)$ | 3.61±0.70 | 0.031±0.003 | 0.155±0.091 |
| $m_{3\min}$ $(M_\odot)$ | 7.33±0.89 | 0.78±0.03 | 1.48±0.37 |
| $a_{3\max}$ (AU) | 15.45±2.12 | 9.98±0.52 | 12.55±3.99 |

where $E$ is the epoch number, $\Delta JD_0$ and $\Delta P_0$ are the correction values for the initial epoch and orbital period of the binary respectively, $\beta$ is the long-term change of the orbital period (d cycle$^{-1}$) and $A\sin(\Omega E+\phi)$ is a sinusoidal term added to fit the cyclic variation. The fitting parameters are listed in the second column of the upper part of Table 2. The result of this fitting is shown in Figure 4. In the top panel of Figure 4, the solid line represents a combination of a secular increase and a cyclic period variation, and the dashed line traces the quadratic fit. In the middle panel, residuals from the parabolic fit and its least-squares fit by the sinusoidal term of Equation (2) (solid line) are displayed. The residuals from the whole fit are displayed in the bottom panel. It is easily seen from the bottom panel of Figure 4 that there are periodic changes in those residuals. To detect possible regular trends in the residuals, we next use a quadratic and two cyclical period variations with eccentricity to fit the $(O-C)_2$ diagram. In order to obtain more reliable results, we only include high-precision observations (photoelectric and CCD data) in the fit generated by this second step. With weights from a non-linear fit, the following equation is derived to fit the $(O-C)_2$ curve,

$$O-C \;=\; \Delta JD_0+\Delta P_0 E+\frac{\beta}{2}E^2+\tau_4+\tau_5, \quad (3)$$

where $\tau_4$ and $\tau_5$ are the cyclic change terms caused by the light travel time effect (LTTE) of supposed additional bodies (Irwin 1952):

$$\begin{aligned}\tau \;&=\; A\left[(1-e^2)\frac{\sin(\nu+\omega)}{1+e\cos\nu}+e\sin\omega\right]\\ &=\; A\left[\sqrt{1-e^2}\sin E^*\cos\omega+\cos E^*\sin\omega\right]. \quad (4)\end{aligned}$$

In Equation (4), $A=a_{12}\sin i_3/c$, $a_{12}\sin i_3$ is the projected semimajor axis, $c$ is the speed of light, $e$ is the eccentricity, $\nu$ is the true anomaly in the position of the eclipsing pair's center of mass on the orbit, $\omega$ is the longitude of the periastron of the eclipsing pair's orbit around the third body, and $E^*$ is the eccentric anomaly.

The relation between the eccentric anomaly ($E^*$) and the observed times of light minima is given by Kepler's equation

$$M \;=\; E^*-e\sin E^*=\frac{2\pi}{P_3}(t-T), \quad (5)$$

where $M$ is the mean anomaly, $T$ is the time of periastron passage, $P_3$ is the period of a supposed third body, and $t$ is the observed times of light minima. The third and fourth columns in the top part of Table 2 list the results of the fit. Figure 5 shows the $(O-C)$ diagrams fitted with these parameters. The $(O-C)_2$ diagram plots the residuals from the fitting of the first step, as displayed in the top panel of Figure 5. The solid line refers to a combination of a quadratic and two cyclical period changes in eccentricity. The downward parabolic change here could be considered as a small correction to the upward parabolic change of the first step. Additionally, lower-precision observations (photographic and visual data) are also drawn in the plot for comparison. The $(O-C)_3$ curve described by the $\tau_4$ and $\tau_5$ terms of Equation (3) (solid line), after removing the other terms, is presented in the middle panel. Residuals of the fit with Equations (3)–(5) are shown in the bottom panel, where no regularity can be found indicating that our calculation gives a good fit to the $(O-C)_2$ diagram.

The $\tau_4$ and $\tau_5$ terms in Equation (3) suggest there are two periodic variations with eccentricities of 0.29 and 0.81 respectively, which are more easily seen in Figure 6.

## 5 CONCLUSIONS AND DISCUSSION

The first observations of the well-known Algol-type binary TW Dra were taken from the surface of the Moon and combined with other historical data. In this paper, we present the near-UV light curve of TW Dra. Photometric solutions with a small third light were obtained. The solutions confirmed that TW Dra is a semi-detached binary where the secondary star fills its Roche lobe. The mass ratio of 0.47 and a high inclination of $86.68^\circ$ are obtained,

which are close to the spectral values given by Tkachenko et al. (2010).

Based on times of light minima spanning more than a century, $(O-C)$ diagrams of TW Dra are constructed. We analyze the complex changes of $(O-C)$ diagrams in two steps. In step 1, a parabolic-plus-one pure cyclic variation pattern is used to fit the general changes seen in the $(O-C)$ curve. It is found that the residuals from the whole fit display obvious changes. The upward parabolic trend indicates that the orbital period of TW Dra is increasing at a rate of $\dot{P} = +3.39 \times 10^{-6}$ d yr$^{-1}$, which could be explained as mass transfer from the secondary component to the primary one at a rate of $6.8 \times 10^{-7}\ M_{\odot}$ yr$^{-1}$. The sinusoidal change with a period of 116.04 yr and a semi-amplitude of 0.2108 d are obtained.

In step 2, parabolic-plus-two cyclic variations with eccentricity are finally adopted to fit the residuals obtained in step 1. The downward parabolic change could be a small correction to the upward one from step 1. It is found that the residuals from step 1 show two cyclic oscillations with eccentricities (i.e., $P_4 = 22.47$ yr and $A_3 = 0.0145^{\rm d}$, and $P_5 = 37.27$ yr and $A_4 = 0.0346^{\rm d}$), where the two periods are in a simple ratio of $3:5$.

Cyclical period changes are usually explained as either the magnetic activity cycles (Applegate 1992) or the LTTE (Frieboes-Conde & Herczeg 1973; Chambliss 1992; Borkovits & Hegedues 1996; Liao & Qian 2010b). Our calculations suggest that the three cyclical period changes of TW Dra cannot be interpreted by the Applegate mechanism. Therefore, based on the reliable orbital elements given by Tkachenko et al. (2010), we calculate parameters describing the orbit of potential additional bodies in the TW Dra system, and list them in the lower part of Table 2. The two possible circumbinary companions derived from step 2 may be in a simple $3:5$ orbit-rotation resonance. According to Allen's tables (Drilling & Landolt 2000), the largest mass companion obtained from step 1 corresponds to a $\sim$ B3 star. However, so far no spectral lines have been found. This may imply that the visual component ADS 9706B itself is a binary system, and the longest cyclical variation may be caused by a disturbance from component B orbiting A (TW Dra). This is similar to quadruple systems VW LMi (Pribulla et al. 2008) and HT Vir (Liao & Qian 2010a). If this conjecture is true, TW Dra itself is a binary in a possible sextuple system with the configuration (1+1)+(1+1)+(1+1), which further suggests that multiplicity is a common phenomenon in close binaries.

**Acknowledgements** The study is supported by the Key Research Program of Chinese Academy of Sience (KGED-EW-603), the National Natural Science Foundation of China (Nos. 11403095, 11133007 and 11325315), the Yunnan Natural Science Foundation (2014FB187), the Science Foundation of Yunnan Province (Grant No. 2012HC011), and the Strategic Priority Research Program "The Emergence of Cosmological Structures" of the Chinese Academy of Sciences (Grant No. XDB09010202). The new observations of the system were obtained by the Lunar-based Ultraviolet Telescope (LUT), and we thank members of the LUT team.

## References

Applegate, J. H. 1992, ApJ, 385, 621
Baglow, R. L. 1952, Publications of the David Dunlap Observatory, 2
Borkovits, T., & Hegedues, T. 1996, A&AS, 120, 63
Bozic, H., Nemravova, J., & Harmanec, P. 2013, Information Bulletin on Variable Stars, 6086
Cao, L., Ruan, P., Cai, H., et al. 2011, Science China Physics, Mechanics, and Astronomy, 54, 558
Chambliss, C. R. 1992, PASP, 104, 663
Drilling, J. S., & Landolt, A. U. 2000, Normal Stars, Allen's Astrophysical Quantities, ed. A. N. Cox (New York: AIP Press; Springer), 388
Frieboes-Conde, H., & Herczeg, T. 1973, A&AS, 12, 1
Giuricin, G., Mardirossian, F., & Predolin, F. 1980, Ap&SS, 73, 389
Irwin, J. B. 1952, ApJ, 116, 211
Liao, W.-P., & Qian, S.-B. 2010a, PASJ, 62, 521
Liao, W.-P., & Qian, S.-B. 2010b, MNRAS, 405, 1930
Meng, X.-M., Cao, L., Qiu, Y.-L., et al. 2015, Ap&SS, 358, 24
Papoušek, J., Tremko, J., & Vestešník, M. 1984, Folia Fac. Sci. Nat. Univ. Purkynianae Brun., Phys., Tomus 25, Opus 4, 64, 25
Pickering, E. C. 1910, Harvard College Observatory Circular, 159, 3
Popper, D. M. 1989, ApJS, 71, 595
Pribulla, T., Baluďanský, D., Dubovský, P., et al. 2008, MNRAS, 390, 798
Qian, S. B., & Boonrucksar, S. 2002, New Astron., 7, 435
Smith, B. 1949, ApJ, 110, 63
Tkachenko, A., Lehmann, H., & Mkrtichian, D. 2010, AJ, 139, 1327
van Hamme, W. 1993, AJ, 106, 2096
Van Hamme, W., & Wilson, R. E. 2007, ApJ, 661, 1129
Walter, K. 1978, A&AS, 32, 57
Wang, J., Cao, L., Meng, X.-M., et al. 2015, RAA (Research in Astronomy and Astrophysics), 15, 1068
Wen, W.-B., Wang, F., Li, C.-L., et al. 2014, RAA (Research in Astronomy and Astrophysics), 14, 1674
Wilson, R. E., & Devinney, E. J. 1971, ApJ, 166, 605
Wilson, R. E. 1979, ApJ, 234, 1054
Wilson, R. E. 1990, ApJ, 356, 613
Wilson, R. E. 2008, ApJ, 672, 575
Wilson, R. E., Van Hamme, W., & Terrell, D. 2010, ApJ, 723, 1469
Wilson, R. E. 2012, AJ, 144, 73
Wolf, M. 1990, Journal of the American Association of Variable Star Observers (JAAVSO), 19, 12
Zejda, M., Mikulášek, Z., & Wolf, M. 2008, A&A, 489, 321
Zejda, M., Wolf, M., Slechta, M., et al. 2010, arXiv:1012.5679
Zhang, X. B., Luo, C. Q., & Fu, J. N. 2013, ApJ, 777, 77